LM-07K001a
March 19, 2007

Spectral Control for Thermophotovoltaic Energy Conversion

PM Fourspring, DM DePoy

NOTICE

Spectral Control for Thermophotovoltaic Energy Conversion

P. M. Fourspring and D. M. DePoy
Advanced Concepts – Advanced Technology
Advanced Reactors Program
KAPL, Inc., a Lockheed Martin Company

Report Number: ARP-AC-1326-PMF-E1

October 2006

This Page Intentionally Blank

TABLE OF CONTENTS

Page

This Page Intentionally Blank

INTRODUCTION

The energy source for thermophotovoltaic energy conversion is a net flux of photons between two surfaces at different temperatures as shown in Figure 1.

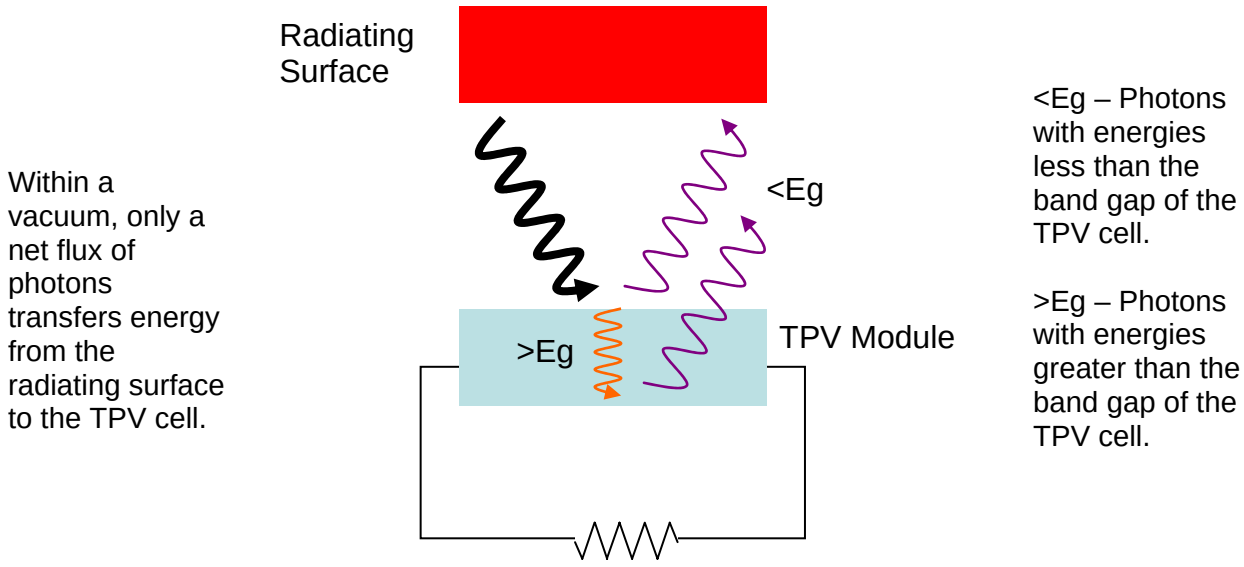

Figure 1: Simplified Thermophotovoltaic Energy Conversion Configuration

Typically these photons are both spectrally and directionally dispersive depending on the materials and geometry of the interacting surfaces. This spectral and directional dispersion, modeled as blackbody radiation, has a significant impact on spectral control device design and overall TPV system efficiency. The wavelength (λ) and radiator temperature (T_h) dependence of radiation from a blackbody is defined by Planck's spectral distribution of emissive power:

$$N(\lambda, T_h) = \frac{2\pi hc^2}{\lambda^5} \cdot \left[\exp\left(\frac{hc}{k_B \lambda T_h} \right) - 1 \right]^{-1} \quad \textbf{Equation 1}$$

where h is Planck's constant, k_B is Boltzman's constant, and c is the speed of light.

Figure 2 compares the spectral distribution of the energy flux for solar radiation 10,895F (6035C) incident at the Earth's surface to a blackbody source at 1750F (954C). The lower temperature TPV blackbody source shows significantly longer average wavelength content (i.e., lower energy) compared to the solar source. In addition, the blackbody spectrum for 1750F (954C) radiator temperature covers a much broader spectral range compared to the solar spectrum. About 95% of the radiated power from a 1750F (954C) blackbody is contained in the wavelength range from 1-10μm compared to the wavelength range from 0.2-2μm for the solar spectrum. The large spectral range of a TPV blackbody radiator necessitates a very wide (~2-10μm) reflection bandwidth for cold side spectral control technologies and/or a very wide

suppressed emission bandwidth for hot side spectral control technologies. This requirement imposes significant constraints on spectral control design and performance from a materials selection viewpoint. For example, front surface filter materials must have very low absorption (extinction coefficient < 0.001) over the spectral range of 1μm to greater than 10μm in order to achieve high transmission of high energy, above band gap photons and high reflection of low energy, below band gap photons.

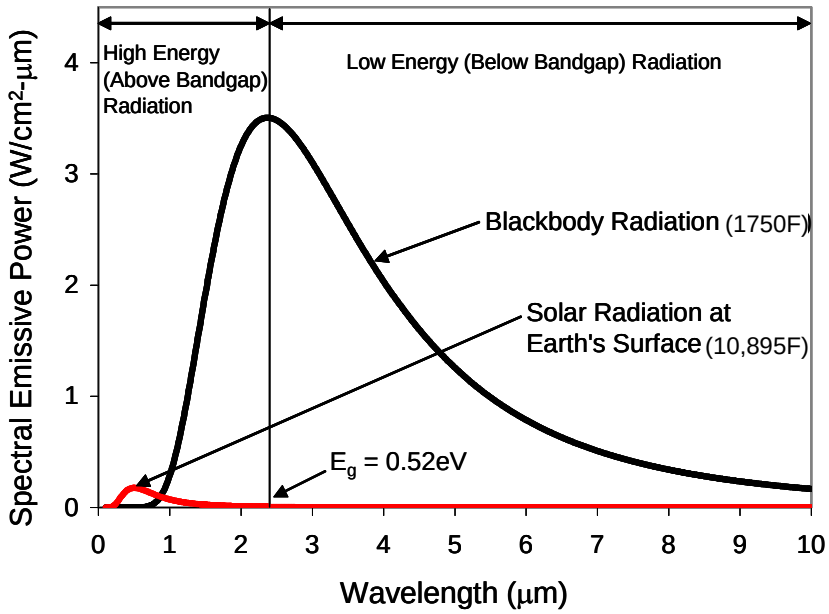

Figure 2: Comparison of Solar and TPV Spectrum

It is important to note that photons are incident on the TPV cell or filter (if applicable) surface from all angles of incidence. The angular dispersion of photons incident on the TPV cold side from a Lambertian TPV radiator surface in an infinite flat plate geometry follows a $\sin\theta \cdot \cos\theta$ dependence (Reference (1)) where θ is the angle of incidence. As shown in Figure 3, this dependence has a peak value at 45°, compared to the near-normal solar spectrum (the result of the large Earth-sun separation). The large angular dispersion of the blackbody TPV source complicates spectral control design and performance in several ways:

- Interference-based filters depend on the optical path length of filter layers, which in turn depends on the angle of photon incidence. The large photon angular dispersion (0^o-90^o) leads to a performance compromise for a fixed filter design.

- The high angular dispersion of incident photons, together with non-specular reflections, lead to the potential for optical frustration, (i.e., trapping and multiple internal reflections within the high refraction index layers of the TPV cell/filter). Frustration can be a major parasitic absorption loss process even for near-zero absorption materials because of the long path lengths.

- At incidence angles greater than 70° (which represent ~12% of the TPV blackbody photon population), the reflection probability increases as predicted from Fresnel's laws ($R \propto \sin^2\theta$). High angle reflection limits the transmission of above-bandgap energy and lowers TPV surface power density.

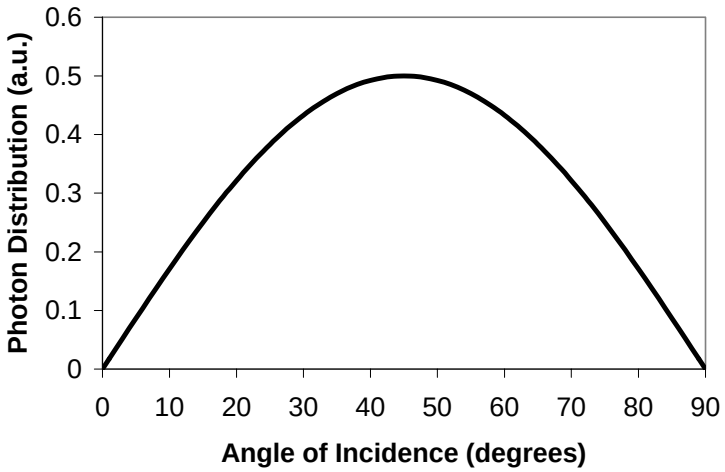

Figure 3: Photon Distribution as a Function of Angle of Incidence

Thermophotovoltaic cells can only convert a subset of the net flux of incident photons. Specifically, photons with energies greater than the band gap of the TPV cell can create electricity; while photons with energies less than the band gap will create parasitic heat if absorbed. Therefore, the useful radiant energy for conversion is a fraction of the total radiant energy. For example, only about 16 percent of the radiant energy can be converted to electricity for a 1750F (954C) radiator temperature and a 0.60 eV band gap TPV cell. The fraction of usable above-band gap energy as a function of TPV cell band gap is shown in Figure 4 for a 1750F (954C) radiator temperature. Ideally, this unconvertible energy should be suppressed from being emitted from the radiator or reflected back to the radiator (recuperated) in order to maximize TPV efficiency.

Without spectral control, TPV energy conversion performance suffers dramatically. Using a simplified expression, TPV efficiency equals to the product of cell efficiency and spectral efficiency (defined later) as follows:

$$\eta_{TPV} = \eta_{Cell} \times \eta_{Spectral} \qquad \textbf{Equation 2}$$

The net conversion efficiency for a 30 percent efficient TPV cell with a 0.60eV band gap and no spectral control would be only 5 percent (30% * 16% = 5%) for a 1750F (954C) radiator temperature. On the other hand, a 75 percent efficient[1], spectral control configuration would yield a net efficiency of 23 percent (30% * 75% = 23%) for the same TPV cell.

[1] As will be presented later, 75% spectral efficiency has been achieved using tandem filters.

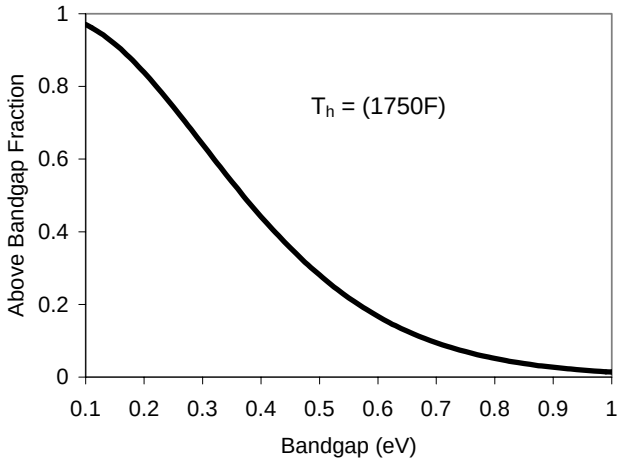

Figure 4: Comparison of Usable, Above Band Gap Energy Fraction with Band Gap for a 1750F (954C) Radiator Temperature

The solution is to modify the net flux of photons so that only above band gap photons reach the TPV cell. Ideally, TPV energy conversion systems should use material structures with surface and bulk optical properties that emit only convertible photons and suppress non-convertible photons from the radiating side or perfectly transmit convertible photons and reflect non-convertible photons that reach the TPV cell. Figure 5 shows ideal spectral performance for radiating surface and the TPV module.

In reality, the current TPV energy conversion systems use material structures for the radiating surfaces that maximize the emission of convertible photons with little or no suppression of the emission of unconvertible photons. As a result, the net radiant flux between the radiating surface and the TPV module includes both convertible and unconvertible photons. Consequently, TPV energy conversion system must include material structures that reflect (or recuperate) the unconvertible photons that reach the front surface of the TPV module to minimize parasitic absorption and at the same time transmit the convertible photons that reach the front surface of the TPV module for conversion to electricity.

Spectral control is the selection, design, and development of material structures used for TPV energy conversion systems that maximize the net flux of convertible (above band gap) photons and recuperate (or reflect) any net flux of unconvertible (below band gap) photons back to the radiating surface. The focus of this selection, design, and development for TPV spectral control is the manipulation of the spectral emittance, reflectance, and transmittance properties of both the radiating surface and the TPV module.

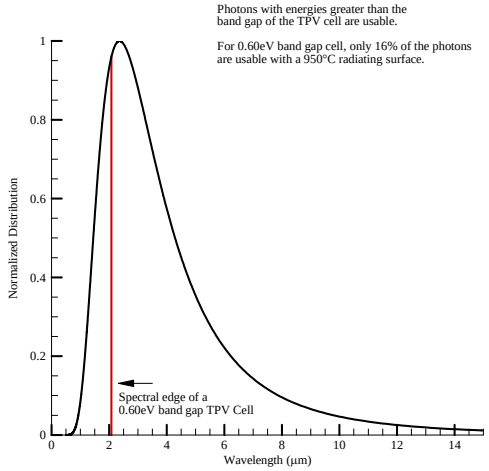

(a)

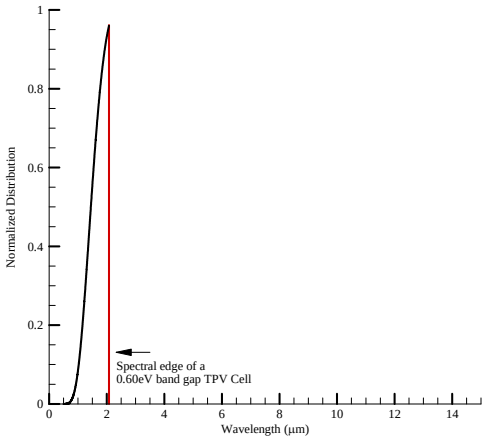

Ideal radiator surface spectral control: emission of only convertible photons with suppression of non-convertible photons

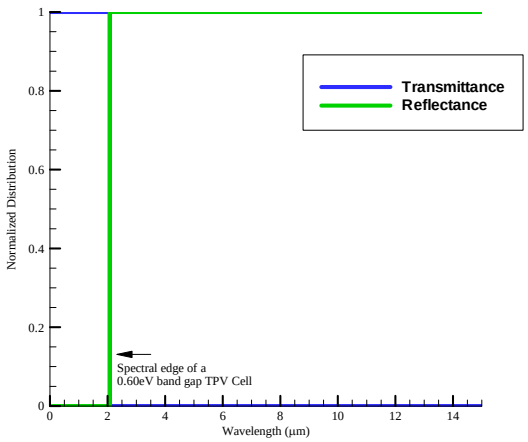

Ideal TPV module spectral control: transmittance of only convertible photons with reflectance of non-convertible photons

(b)

Figure 5: Spectral Distribution Reaching the TPV Module <u>without</u> Spectral Control (a) and <u>with</u> Ideal Spectral Control (b)

Background

In the mid 1980s, spectral control was identified as an enabling technology for TPV energy conversion (References (1, 2)). Since then, the development of various spectral control technologies has occurred in parallel with the development of TPV cell technology. Table 1 summarizes the spectral control options that have been postulated.

Table 1 Elements of TPV Energy Conversion (Spectral Control Elements are Shaded)

Radiator	• Selective and Textured Radiators • Filtered Radiator • 3-D Photonic Crystal Structure Radiator
Gap	↑ **Hot Side** ↓ **Cold Side**
Front Surface	• Interference Filter, Plasma Filter, or Combination (Tandem Filter) • Frequency Selective Surface (FSS) filter • 3-D Photonic Crystal Structure Filter
TPV Cell	
Back Surface	• Metallic Back Surface Reflector (BSR)

For the radiator side or hot side of the gap, selective and textured radiators represent the use of bulk materials with intrinsic, spectral emittance properties at the required temperature (usually greater than 1832F (1000C) (References (3-11)). A filtered radiator enhances the intrinsic spectral emittance by applying numerous thin layers on the bulk material (Reference (5)). A three dimensional photonic crystal structure radiator has been postulated for use as either an engineered bulk material or a filter on a bulk material (Reference (12)). As a filter the 3-D photonic crystal structure would represent an extension of the filtered radiator approach (a 1-D photonic crystal) with additional dimensions.

On the front surface of the cold side, several filter options exist. Edge pass (short pass) optical filters use thin layers of materials to take advantage of the interference effect and to get desired optical properties. Plasma filters use a highly doped, semiconductor layer to achieve optical properties with a reflectance region like a metal and a low absorption region like an insulator. A tandem filter is an edge pass filter in series with a plasma filter (References (13-17)). Another front surface option is frequency selective surface (FSS) filters that selectively reflect and transmit incident electromagnetic radiation via currents induced in a periodic array of metal (Reference (18)). A 3-D photonic crystal structure extends the use of the interference effect to three dimensions (Reference (19)).

Finally, for the back side, a metallic reflector refers to a highly reflective material applied to the backside, opposite to the illumination side, of a TPV cell.

TECHNICAL BASIS

For any energy conversion system, the efficiency of and the volume or mass associated with the conversion process are central. The merit functions for TPV spectral control, spectral efficiency ($\eta_{spectral}$) and above band gap transmission ($T_{>Eg}$), capture the spectral control performance that relates to the conversion efficiency and power density of a TPV energy conversion system. The spectral efficiency is the ratio of the integrated above band gap power absorbed in the active region of the TPV cell to the total power absorbed in the TPV cell. The integrated, above band gap transmission is the ratio of the integrated above band gap power absorbed by the TPV cell to the above band gap power radiated from a blackbody. In other words, the fraction of above band gap power from a blackbody that is transmitted to the active region of the TPV cell reduced by radiator emittance less than one, cold side reflectance, and filter absorptance, if any. Specifically, these merit functions are defined as follows, assuming specular surfaces in an infinite parallel plate configuration:

$$\eta_{spectral} = \frac{\int_0^{\frac{\pi}{2}} \int_0^{\lambda_g} \varepsilon_{eff}(\lambda,\theta,T_{rad}) \frac{T(\lambda,\theta)}{1-R(\lambda,\theta)} N(\lambda,T_{rad}) \sin\theta\cos\theta d\lambda d\theta}{\int_0^{\frac{\pi}{2}} \int_0^{\infty} \varepsilon_{eff}(\lambda,\theta,T_{rad}) N(\lambda,T_{rad}) \sin\theta\cos\theta d\lambda d\theta} \quad \textbf{Equation 3}$$

$$T_{>Eg} = \frac{\int_0^{\frac{\pi}{2}} \int_0^{\lambda_g} \varepsilon_{eff}(\lambda,\theta,T_{rad}) \frac{T(\lambda,\theta)}{1-R(\lambda,\theta)} N(\lambda,T_{rad}) \sin\theta\cos\theta d\lambda d\theta}{\int_0^{\frac{\pi}{2}} \int_0^{\lambda_g} N(\lambda,T_{rad}) \sin\theta\cos\theta d\lambda d\theta} \quad \textbf{Equation 4}$$

Where:

$T(\lambda,\theta)$ is the transmittance of the cold side as a function of wavelength and angle of incidence,

$R(\lambda,\theta)$ is the reflectance of the cold side as a function of wavelength and angle of incidence. $R(\lambda,\theta)$ can be the reflectance of any of the following:

- a front surface filter on a TPV cell (with or without a BSR),
- a TPV cell (with or without a BSR) with an antireflection coating,
- a bare TPV cell (with or without a BSR).

Since $T(\lambda,\theta)$ is equal to $1 - R(\lambda,\theta) - A(\lambda,\theta)$, $T(\lambda,\theta) / 1 - R(\lambda,\theta)$ in the numerator becomes one when no absorption ($A(\lambda,\theta)$) in the front surface filter exists or no front surface filter exists (as with a cell with a back surface reflector only),

λ is wavelength,

λ_g is the wavelength corresponding to the band gap (E_g) of the TPV cell,

$N(\lambda,T_{rad})$ is Planck's blackbody spectral distribution of emissive power as a function of wavelength and temperature,

θ is the angle of incidence of incoming photons,

T_{rad} is the radiator temperature,

$\varepsilon_{eff}(\lambda,\theta,T_{rad})$ is the effective cavity emittance for infinite, parallel plates as follows:

$$\varepsilon_{eff}(\lambda,\theta,T_{rad}) = \frac{1}{\frac{1}{\varepsilon_{rad}(\lambda,\theta,T_{rad})} + \frac{1}{1-R(\lambda,\theta)} - 1}$$ **Equation 5**

$\varepsilon_{rad}(\lambda,\theta,T_{rad})$ is the radiator emittance as a function of wavelength, angle, and temperature

Note that $\varepsilon_{eff}(\lambda, \theta, T_h)$ simplifies to 1 - $R(\lambda,\theta)$ for the ideal case of a blackbody radiator ($\varepsilon_{rad}(\lambda,\theta,T_h) = 1$), and that the $T(\lambda,\theta)$ /(1- $R(\lambda,\theta)$) term in Eq. (2) and (3) accounts for parasitic absorption of above bandgap photons in a front surface filter (if applicable). It is also useful to define the integrated below bandgap effective emissivity, $\varepsilon_{<Eg,eff}$, as follows:

$$\varepsilon_{<Eg,eff} = \frac{\int_0^{\frac{\pi}{2}} \int_{\lambda_g}^{\infty} \varepsilon_{eff}(\lambda,\theta,T_h) N(\lambda,T_h) \sin\theta\cos\theta d\lambda d\theta}{\int_0^{\frac{\pi}{2}} \int_{\lambda_g}^{\infty} N(\lambda,T_h) \sin\theta\cos\theta d\lambda d\theta}$$ **Equation 6**

These merit functions are aggregate, energy weighted measures of TPV spectral performance and have been shown to correlate with the independently measured efficiency and power density of a combined TPV cell and spectral control configuration (References (20, 21)). The performance, as captured in the merit functions, is dependent on the available energy as a function of wavelength (according to the Plank distribution) and incident angle. As a result, reflectance at a wavelength of 3µm and a 45° incident angle is much more important than performance at a wavelength of 15µm and a 45° incident angle. Spectrally, about 96% of the available energy is between 1.25-13.5µm for a radiator temperature of 1750F (954C). Directionally, the available energy is a symmetric distribution about a peak at 45° incident angle (See Figure 3).

Examination of Equation (3) indicates that high spectral efficiency requires a spectral control technology with very low, integrated below band gap effective emissivity, high integrated above band gap transmission, and low parasitic absorption of above band gap photons in the filter (if applicable). Figure 6 shows the relationship between spectral efficiency and integrated below band gap effective emissivity for a radiator temperature of 1750F (954C), an integrated above band gap transmission of 85%, a 0% above band gap parasitic filter absorption, and TPV cell band gaps of 0.4 eV, 0.5 eV, 0.6 eV, and 0.7 eV. As shown in Figure 6, spectral efficiency is a strong function of integrated below band gap emissivity and TPV cell band gap. Higher integrated below band gap effective emissivity results in higher parasitic absorption and lower spectral efficiency. Spectral efficiency is higher for lower band gap TPV cells because the

above band gap fraction is higher (Figure 4). In order to achieve spectral efficiencies of 85%, integrated below band gap emissivity must be less than 12%, 6%, 3%, and 1.6% for 0.4 eV, 0.5 eV, 0.6 eV, and 0.7 eV TPV cell band gap, respectively.

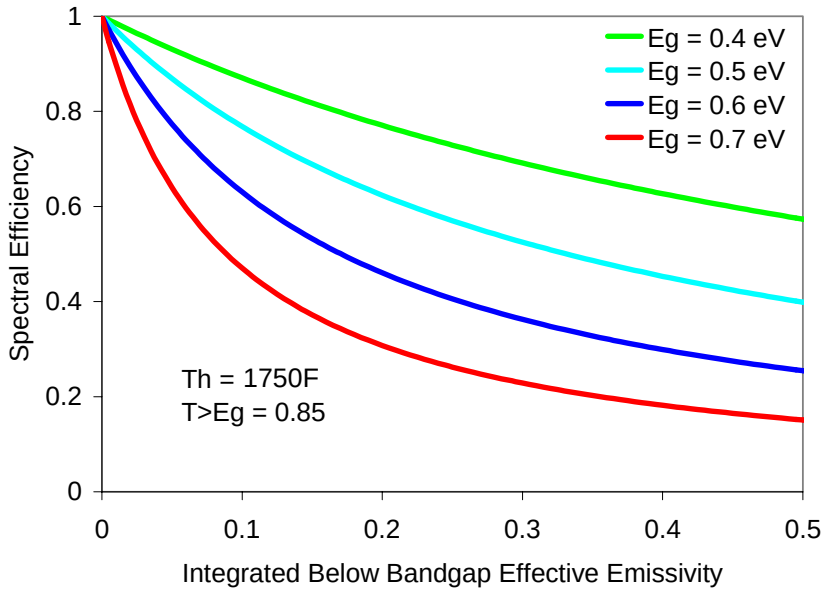

Figure 6: Comparison of Spectral Efficiency with Integrated Below Band Gap Effective Emissivity

SPECTRAL CONTROL

The following spectral control configurations have had significant development:

- Front surface, tandem filters,
- Front surface, frequency selective surface filters,
- Metallic back surface reflectors, and
- Selective, textured, and filtered radiating surfaces.

Spectral control configurations that involve 3-D photonic crystal structures are in the beginning stages of development and comparisons with the spectral control configurations in the previous list is premature.

Front Surface Spectral Control

Front surface spectral control using tandem filters has achieved the highest spectral efficiency of any spectral control configuration to date (References (22-24)). In contrast, both the modeled and predicted performance of frequency selective surfaces as front surface, spectral control have achieved significantly lower spectral efficiencies and above band gap transmission

performance than tandem filters (Reference (25)). The performance of the third option, photonic crystal structures, listed in Table 1 has yet to be shown but may provide better performance than tandem filters (References (19)).

Tandem Filters

A tandem filter is a combination of a plasma filter and an interference filter (References (15-17, 24, 26)), as shown in Figure 7. The interference filter provides high transmission of above band gap photons, high reflection of below band gap photons from the band gap wavelength to approximately 6μm, and a sharp transition from high transmission to high reflection at or near the band gap wavelength. The plasma filter provides low absorption for above band gap photons and high reflection for below band gap photons with wavelength greater than ~6μm. Figure 7 also illustrates the performance of the tandem filter concept by showing the spectral response of the interference filter, the plasma filter, and the combination of the two as a tandem filter.

The plasma filter consists of a heavily doped (~$5x10^{19}$ cm^{-3}) n-type (doped with Te) layer of $InP_{0.75}As_{0.25}$ epitaxially grown using organo-metallic vapor phase epitaxy (OMVPE) onto a double side polished InP substrate (References (27, 28)). This plasma filter has a plasma wavelength of 4.5-5μm. Essentially, the plasma filter acts like a dielectric in the short wavelength above band gap spectral region and acts like a metal in the long wavelength spectral region.

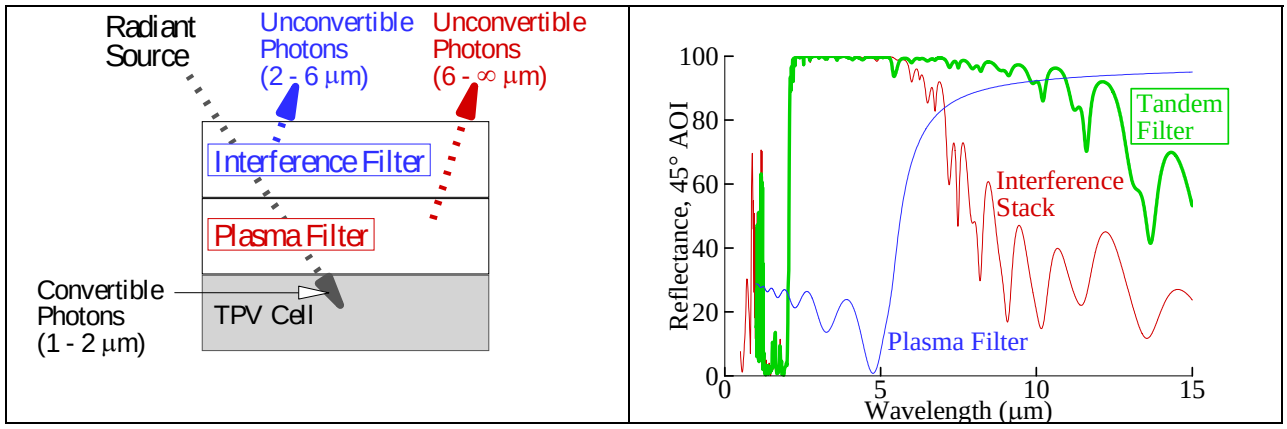

Figure 7: Tandem Filter Concept

The interference filter consists of a multilayer stack of dielectric materials. Sb_2Se_3 (n~3.4) is used as the high index of refraction material and YF_3 (n~1.5) is used as the low index of refraction material. The development of Sb_2Se_3 as a high index of refraction interference filter material is a key program achievement that has enabled high TPV spectral performance. Sb_2Se_3 provides a high index of refraction (~3.4) and a very low extinction coefficient (<0.0001) across the entire spectral range (from 0.85μm to greater than 30μm).

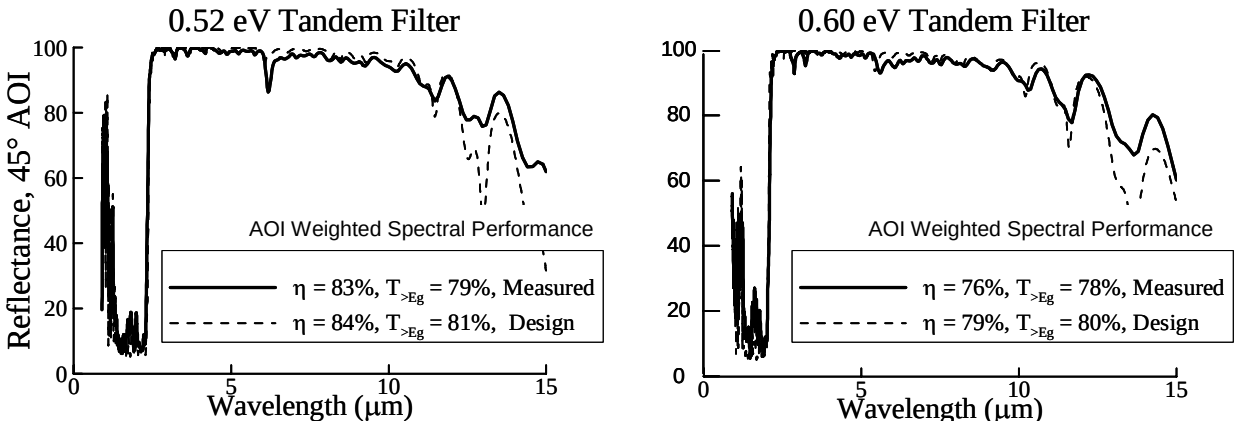

Figure 8: Current Spectral Performance of Front Surface, Tandem Filters

Figure 8 shows the measured and predicted reflection (45° incident angle) versus wavelength of tandem filters fabricated for 0.52 eV and 0.60 eV TPV cells. The measured results are in excellent agreement with predictions made using OptiLayer™ thin film design software. Specifically, the measured results show very high reflectivity in the below bandgap region, minimal edge shift with angle of incidence, and sharp transition at the bandgap wavelength. Sb_2Se_3/YF_3 tandem filters represent the highest spectral performance achieved to date for TPV spectral control. Specifically, tandem filters have achieved spectral efficiencies of ~83% for a 0.52eV band gap and ~76% for a 0.60eV band gap for a 1750F (954C) radiator temperature. Moreover, a 0.60eV band gap tandem filter enabled a measured, TPV conversion efficiency of 22%, the greatest TPV conversion efficiency to date (Reference (29)).

The Sb_2Se_3 material within the interference filter limits, however, the operating temperature of the tandem filter. A single layer of Sb_2Se_3 transforms from an amorphous material to a crystalline material at approximately 293F (145C) after a few minutes as shown in Figure 9. This transformation results in an unacceptable increase in absorption. Figure 10 shows the impact of the increased absorption for a Sb_2Se_3 based tandem filter at 212F (100C) for about 330 hours. This figure also shows that at 176F (80C) after about 1150 hours no change in the performance of a Sb_2Se_3 based tandem filter occurred.

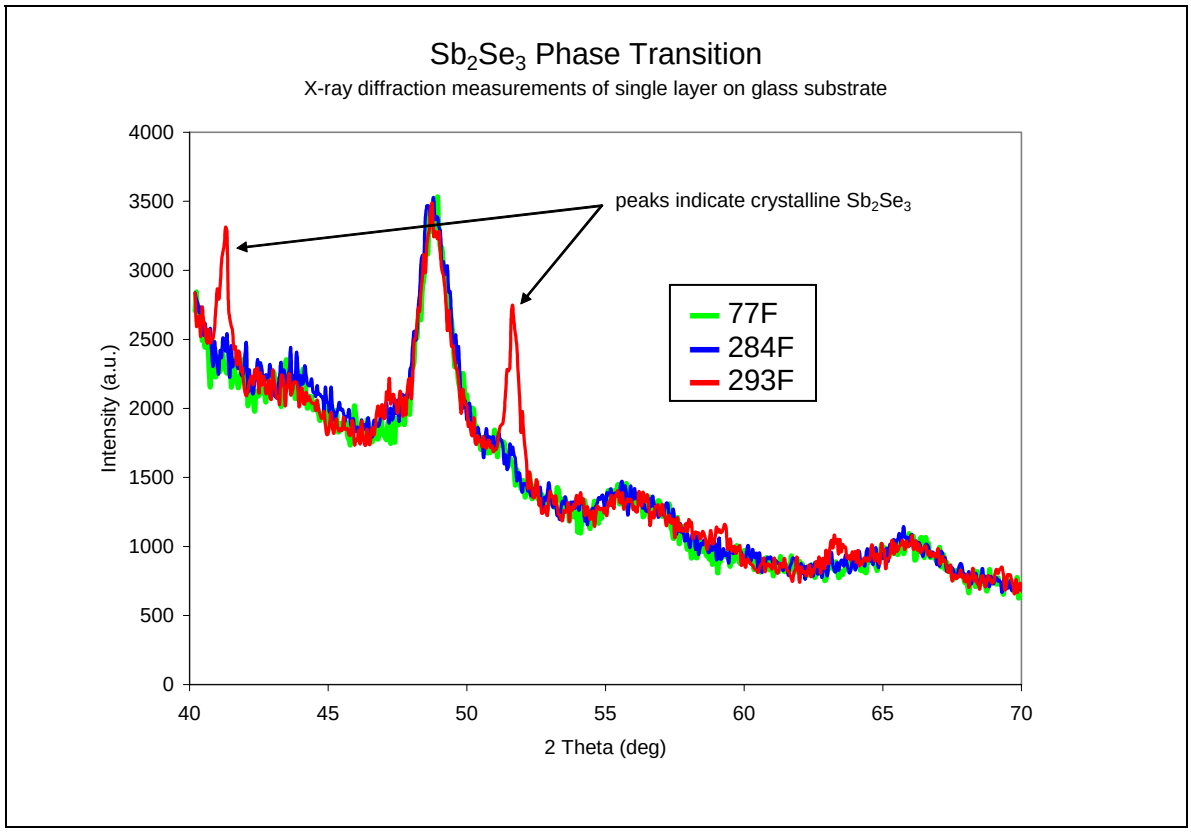

Figure 9: Temperature Stability of Single Layers Sb_2Se_3 Using X-Ray Diffraction

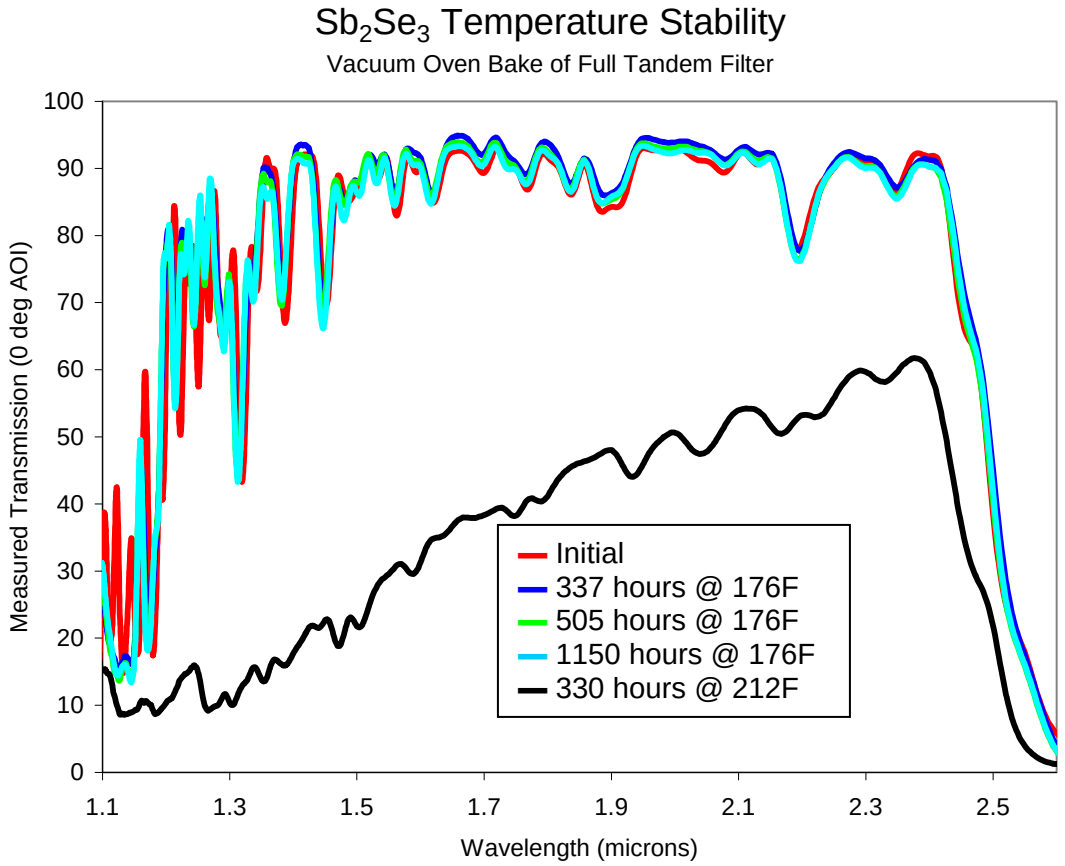

Figure 10: Temperature Stability of Sb_2Se_3 Based Tandem Filters

Given the temperature stability limitation of Sb_2Se_3, alternative materials were sought to replace the Sb_2Se_3. To be sure, a back surface reflector could be used without a front surface, tandem filter and, therefore, eliminate the associated temperature stability limitation. However, as will be described later, the efficiency performance of a back surface reflector is about 25 percent less than a tandem filter.

Two alternative materials have been identified, GaTe and Sb_2S_3, to replace the Sb_2Se_3 in the tandem filter. Similar to the evaluation of Sb_2Se_3, the transformation temperatures of these materials are shown in Figure 11. The GaTe material is the preferred material because it has a higher refractive index (n~3.1) than Sb_2S_3 (n~2.8). Accordingly, fabrication development was focused on GaTe based tandem filters, and numerous GaTe based tandem filters have been fabricated successfully.

However, the refractive index of GaTe is lower than refractive index (n~3.4) of Sb_2Se_3 and therefore, the performance of the GaTe tandem filter designs are expected to be slightly lower (~1-2%) than the comparable performance for the Sb_2Se_3 based tandem filter designs.

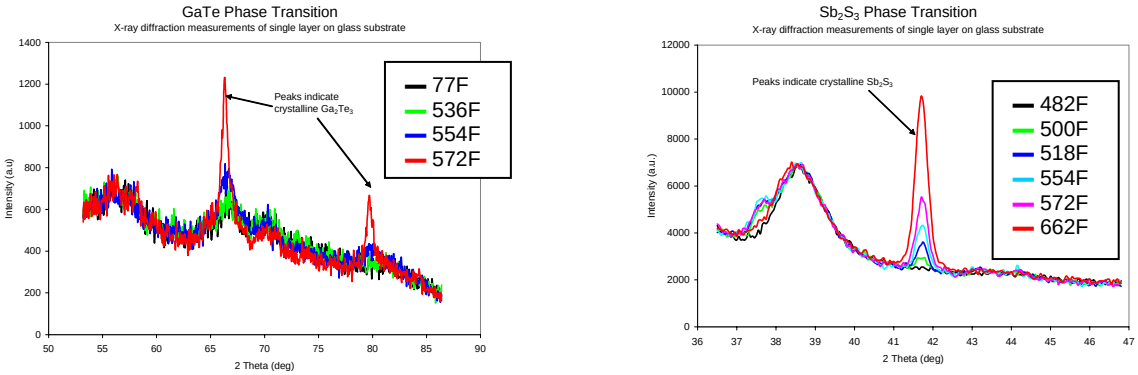

Figure 11: Temperature Stability of Single Layers of GaTe and Sb_2S_3

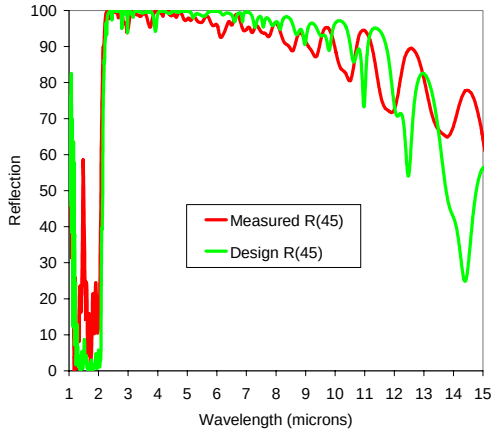

Energy weighted spectral performance:

<u>Measured</u>

$\eta_{spectral}$ = 73%, $T_{>Eg}$ = 73%

<u>Design</u>

$\eta_{spectral}$ = 79%, $T_{>Eg}$ = 81%

(For $T_{radiator}$ = 1750°F (954°C), $\varepsilon_{radiator}$ = 1.0 (all λ))

Figure 12: Performance of GaTe Based Tandem Filters

In the end, Sb_2Se_3 based tandem filters provide the highest spectral efficiency but with the operating temperature limit of about 176F (80C), and GaTe based tandem filters provide slightly lower performance than Sb_2Se_3 based tandem filters but allow an operating temperature of at least 302F (150C). Currently the measured, spectral efficiency of GaTe based tandem filters is about 4% less than the Sb_2Se_3 based tandem filters. This difference may decrease with additional development.

Frequency Selective Surfaces

A frequency selective surface (FSS) is a two-dimensional periodic array of electromagnetic scattering elements (metal holes or patches) with wavelength selective spectral properties that depend on the size, shape, and spacing of the elements (Reference (18)). It has been proposed that an FSS with sub-micron feature size would be a suitable filter for thermal radiation (1-10 μm) in a TPV application (References (30-32)). However, as described below, spectral performance of both fabricated and modeled FSS structures is significantly lower than the tandem filter.

Figure 13 provides a comparison of the measured spectral performance at 11^{o} incident angle and predicted spectral performance at normal incidence of an aluminum ring-aperture FSS. The ring-aperture aluminum FSS structure was fabricated via phase-shift lithography at MIT Lincoln Laboratory (Reference (33)) and modeled using Ansoft Corporation's finite-element High Frequency Structure Simulator (HFSS) code. In general, good agreement is achieved between measured data and simulated results. As shown in Figure 13, the ring aperture FSS exhibits a peak in absorption of approximately 20 percent in the filter pass band for both measured and simulated spectral performance. As described below, this unacceptably high absorption is caused by ohmic losses resulting from induced currents in the FSS metallization.

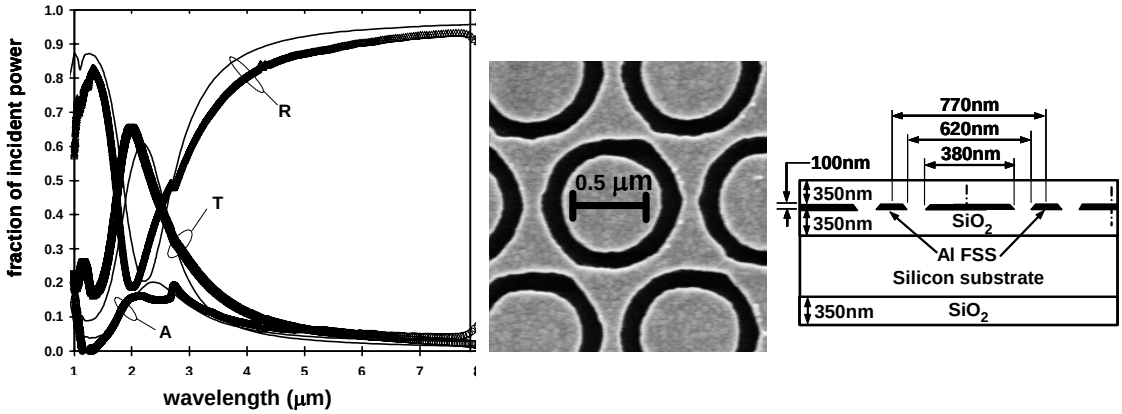

Figure 13: Measured (points) and Modeled (lines) Ring Aperture FSS Spectral Performance (Left), SEM (center) and structure (right)

FSS filters selectively reflect and transmit incident radiation depending on the superposition between the incident field and the scattered field from the induced currents in the metallic FSS. The induced currents are determined by the geometry of the FSS and can be represented by a resonant circuit of inductive, capacitive, and resistive elements (Reference (18)). The resistance is due to the finite conductivity of the metal structure and results in ohmic losses that are measured as absorption in the FSS structure. An FSS modeled as a perfect electrical conductor does not show any absorption. This absorption mechanism is thus intrinsic to FSS

operation given the finite conductivity of the metal, (References (25, 34, 35)) and is particularly detrimental to TPV filter performance because the peak absorption occurs at or near the peak in filter transmission. Physically, the peak absorption is a maximum at the filter resonance because the induced currents reach peak values and the maximum fraction of the FSS metal (i.e., both sides of the filter) participates in the resonant behavior (Reference (35)).

The spectral performance of the ring aperture FSS is compared to the tandem filter in Table 2 assuming a 1750F (954C) radiator and a cell band gap that provides high filter efficiency near the peak of integrated above band gap transmission. The poor relative performance of FSS is predominately due to the relatively slow reflection turn-on of the FSS at the band edge, high above band gap reflection, and the high above band gap absorption. The spectral performance of the fabricated FSS is optimal for a cell with a lower band gap (0.45eV) than the tandem filter (0.52eV). Consequently, the calculated parameters in the table are determined at this lower band gap for a best-case-scenario comparison.

Several FSS design techniques have been explored to mitigate the above band gap absorption (Reference (25)) including: (1) replacing the aluminum metal with silver (higher DC conductivity), (2) reducing the metal area with a wire-mesh design, and (3) mounting an interference filter on a single-layer wire mesh FSS. The only approach that significantly improves the spectral performance is the addition of an interference filter to the wire mesh FSS, which, despite the aggressive assumptions, remains below the tandem filter performance. As shown in Table 2, all of the other cases considered had either significant above band gap absorption or low below band gap reflectivity and hence relatively poor spectral performance.

For computational reasons, FSS structures were modeled only at normal incidence at the most favorable azimuthal (ϕ) orientation for a given FSS geometry. Variation in spectral performance with polar (θ) angle-of-incidence is common for any filter, but variation with azimuthal angle is specific to FSS because of the 2-D periodicity of the FSS array and element shape. Fabricated structures were measured at numerous orientations (both θ and ϕ) (Reference (25)), but for consistency with the modeling, the performance metrics were calculated near normal incidence. The degradation in FSS spectral performance for off-design angles is ignored here, but must be considered in actual TPV applications as the decrement is considerable and unavoidable due to the Lambertian distribution of the radiation. Consequently, the performance metrics in Table 2 are optimistic predictions of FSS performance. An idealized 45°-only spectral performance is also calculated for the tandem filter for better comparison to the FSS structure.

In general, all FSS filters fabricated to date by MIT Lincoln Laboratory and modeled by Lockheed Martin exhibit low above band gap transmission, high absorption in the filter pass band, and significant degradation in spectral performance for off-design angles of incidence (polar and azimuthal). One exception to this is the wire mesh FSS geometry which had low below-bandgap reflectivity. The origin of the pass-band absorption is attributed to ohmic losses in the FSS metallization, and is believed to be inherent—even in a perfectly fabricated structure—as it is the result of the induced currents in the finite conductivity FSS metal. If it is assumed that FSS filters could be optimized for isotropic infrared radiation and if the above band gap reflectivity could be reduced, then the significant absorption in the pass band would still be a fundamental obstacle to incorporating a FSS filter into high-efficiency high-power density TPV spectral control.

Table 2: Comparison of Tandem and FSS Filter Performance [a]

Configuration	Efficiency	Integrated			
		Above Band Gap			Below Band Gap
		Transmission	Absorbtion	Reflectivity	Reflectivity
TPV Filter Goal	85%	85%	3%	15%	97%
Tandem filter[b] (measured)	83%	79%	3%	18%	94%
Tandem filter[c] (calculated)	84%	81%	3%	13%	96%
Ring-aperture FSS[e] (measured)	~48%	~45%	~12%	~43%	~80%
Ring-aperture FSS[d] (calculated)	~50%	~40%	~14%	~46%	~85%
Al Wire-mesh FSS[d] (calculated)	~55%	~80%	~7%	~13%	~68%
Wire-mesh FSS[e] (measured)	~45%	~71%	~5%	~24%	~67%
Wire-mesh FSS[d] w/ Tandem Filter[c] (estimated)	~75%	~66%	~5%	~29%	~93%

a) Parameters calculated for optimal cell bandgap (0.45-0.55eV) and radiator temperature T_{rad} = 954C;
b) Angle-of-incidence weighted;
c) 45° Angle-of-incidence;
d) 0° Angle-of-incidence;
e) 11° Angle-of-incidence

Back Surface Spectral Control

Back surface, metallic reflectors have achieved useful levels of spectral performance but less than the spectral efficiency of front surface, tandem filters. A back surface, metallic reflector or more commonly a back surface reflector (BSR) (Reference (36-38)) reflects (recuperates) below band gap photons that pass through the TPV cell back to the radiating surface through the cell as shown in Figure 14.

The measured spectral performance of a 0.60 eV InGaAs monolithically integrated module (MIM) with a back surface reflector and a single layer Si_3N_4 antireflection coating is shown in Figure 14 for both unprocessed and processed (i.e., addition of grid fingers and trenches needed for the MIM concept) material. The BSR in Figure 14 achieved 55 percent spectral efficiency with ~82 percent above band gap transmission. An in-cavity TPV efficiency measurement of 17 percent has been achieved using 0.6eV InGaAs MIM with a BSR (Reference (21)).

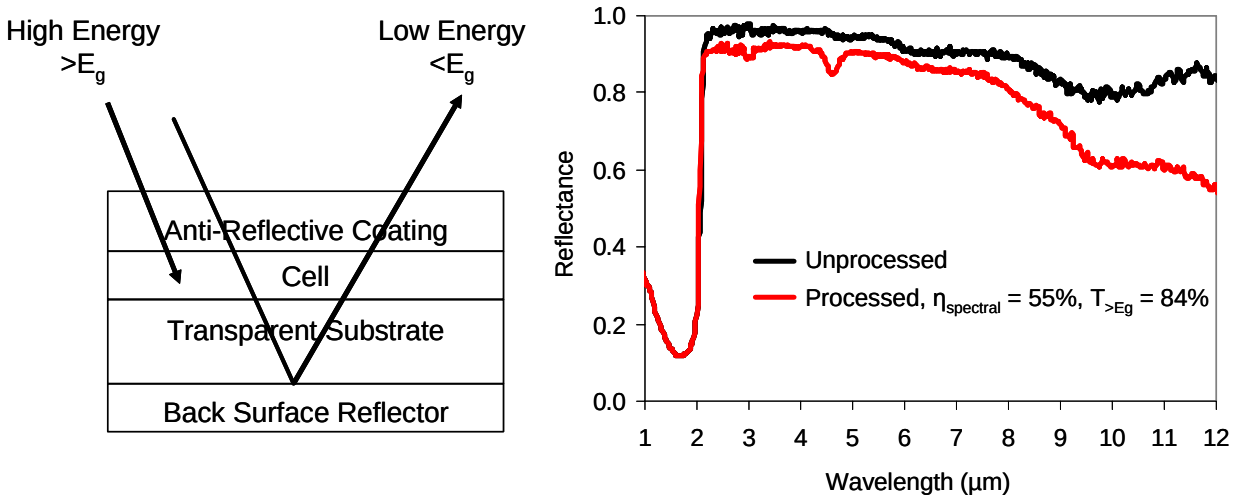

Assumptions: $T_{radiator}$ = 1750°F (954°C), T_{cell} = 50°C, $\varepsilon_{radiator}$ = 1.0

Figure 14: Measured Near Normal Reflectance of Back Surface, Metallic Reflectors

Spectral performance of the BSR concept is primarily limited by free carrier absorption in the TPV diode layers. Free carrier absorption in the diode layers or diode substrate reduces long wavelength reflectivity. Therefore, low diode layer doping and a very low doped semi-insulating substrate (e.g., InP) should be used to maximize BSR spectral performance. Alternatively, in some diode concepts, substrate thinning or removal could be performed to mitigate the absorption caused by a conducting substrate. In most diode architectures, free carrier absorption causes a trade-off between diode and spectral performance (i.e., higher doping in some diode layers improves diode performance at the expense of BSR spectral performance). In addition, as shown in Figure 14, TPV device processing causes light scattering and trapping which results in a further reduction of below band gap reflectance.

The BSR spectral control option has the advantage of being less complicated than a tandem filter and it provides higher integrated above band gap transmission (85% to 90% for BSR compared to ~80% for tandem filters). However, current BSR spectral efficiency is significantly lower than current tandem filter spectral efficiency (~55% for BSR compared to ~75% for tandem filters for the assumptions shown in Figure 14. Diode design and fabrication experience to date indicates that there is little room for improvement of the BSR spectral performance without significantly impacting diode performance.

Radiating Surface Spectral Control

The spectral efficiency and above band gap transmission performance of materials and structures used for radiating surface spectral control has been significantly less than the performance of front surface, tandem filters and less than the performance of back surface reflectors. The performance to date has shown that wavelength selective radiators have spectral efficiencies of about 50% or less.

The considerable development effort to date of selective, textured, or filtered radiator surfaces for TPV energy conversion (Reference (3-11)) has shown the difficulty of achieving the desired spectral emittance performance at high temperatures. Since the radiators inherently operate at high temperatures, the availability of stable materials and structures with the necessary optical properties is limited. Selective radiators (e.g., rare earth oxides) represent the use of bulk materials with intrinsic spectral emittance properties at the required temperature of operation. Surface modification can be used for textured TPV radiators to increase the short wavelength ($E>E_g$) emissivity of a base material with low long wavelength ($E<E_g$) emissivity (e.g., tungsten). A filtered radiator enhances the intrinsic, spectral emittance by applying thin layers on the bulk radiator material. A 3-D photonic crystal structure radiator has been postulated for use as either an engineered bulk radiator material or a filter on a bulk radiator material (Reference (12, 19)).

To equal the performance of current front surface, tandem filters, selective, filtered, textured, or photonic crystal radiator surfaces must achieve a spectral emittance equal to one minus the spectral reflectance of a front surface, tandem filter as shown in Figure 15. This figure shows only the performance at 45° incidence angle. A radiating surface would need to have the high above band gap emittance with a sharp transition to a low emittance in the below band gap spectral region. In addition, this radiating surface would need to achieve the same performance of the front surface, tandem filters at all incidence angles.

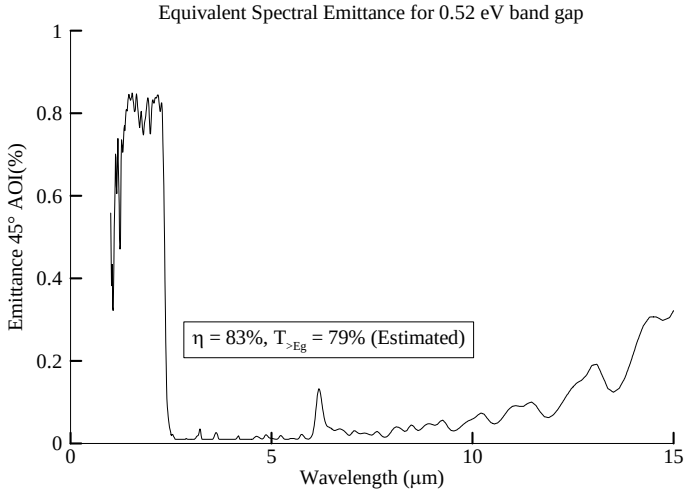

Figure 15: Equivalent Spectral Emittance to Achieve Spectral Performance of Front Surface, Tandem Filters with High Emissivity (~0.8) Radiator

TPV ENERGY CONVERSION SYSTEM DESIGN

The spectral and directional dispersion of photons are important considerations in the design TPV energy conversion systems, as the following discussions suggest.

TPV Band Gap Selection

The selection of the TPV cell band gap is a function of the required performance of a TPV energy conversion system and of the performance of the available spectral control technology.

For a given radiator temperature, spectral control eases as the band gap of the TPV cell decreases. As the band gap decreases, the percentage of usable energy increases and the spectral control technology needs to recuperate less unusable energy. However, TPV cell efficiency decreases, in general, as the band gap of the TPV cell decreases.

Figure 16 presents calculations of TPV efficiency, η_{TPV}, and output power density, P_{out} (W/cm^2), as a function of TPV cell bandgap and integrated below bandgap effective emissivity. TPV efficiency is calculated from:

$$\eta_{TPV} = P_{out}/q_{total} = \eta_{cell} \cdot \eta_{spectral} \cdot \eta_{module} \qquad \textbf{Equation 7}$$

$$\eta_{cell} = QE \cdot F_o \cdot q_0 V_{oc} / E_g \cdot FF \qquad \textbf{Equation 8}$$

where:

q_{total} is the total heat flux absorbed (W/cm^2),
η_{cell} is the TPV cell efficiency,
$\eta_{spectral}$ is the spectral efficiency,
η_{module} is the module efficiency (defined in the next section),
QE is the photon weighted internal quantum efficiency,
F_o is the photon over excitation efficiency,
q_0V_{oc} / E_g is the open circuit voltage efficiency (q_0 is the charge of an electron),
FF is the power usage efficiency or fill factor,

The following assumptions were made in this parameter study:

- integrated above bandgap transmission = 76% (consistent with 90% above bandgap radiator emissivity, 15% above bandgap filter reflectivity, and 2% above bandgap filter absorption)
- radiator temperature = 1750F (954C)
- TPV cell temperature = 122F (50C)
- QE = 95%
- FF = 0.95 x $FF_{Rs=0}$ = 95% of the zero series resistance fill factor
- 10% inactive area with reflectivity as indicated in Figure 16

These assumptions are consistent with the performance of state-of-the-art TPV cells and filters. The following correlation for TPV cell dark current density versus TPV cell bandgap and TPV cell temperature was used in this parameter study:

$$J_o\ (A/cm^2) = 1.583 \times 10^{-5} \cdot e^{2.912\ Eg} \cdot (T_{cell})^3 \cdot e^{-Eg/kB\ Tcell} \qquad \textbf{Equation 9}$$

Equation 9 is based on a correlation from Wanlass (Reference (39)), scaled to be consistent with PC-1D analysis of the projected performance (based on engineering limits) of 0.52eV

InGaAsSb TPV cells (Reference (40)) and 0.60eV InGaAs cells. The following assumptions were used in the PC-1D analyses:

- TPV cell active layer thickness = 2.8 μm
- front and back surface recombination velocity = 10 cm/sec
- Shockley Reed Hall recombination lifetime = 3μs
- Auger recombination coefficient, C = 10^{-28} cm^6/sec

Radiative recombination and photon recycling modeled using an effective radiative recombination coefficient: $B_{eff} = B/\varphi = 2.86 \times 10^{-12}$, where B is calculated using the van Roosbroek-Shockley relationship and the photon recycling factor, φ, is calculated according to Asbeck (Reference (41)) assuming a 100% reflecting back surface.

Figure 16 shows that even low levels of integrated below band gap effective emissivity have a significant effect on TPV efficiency and on the location of the optimum (peak efficiency) TPV cell band gap. Note that efficiency is a weak function of TPV cell band gap near the peak efficiency whereas power density is a strong function of TPV cell band gap in this same range.

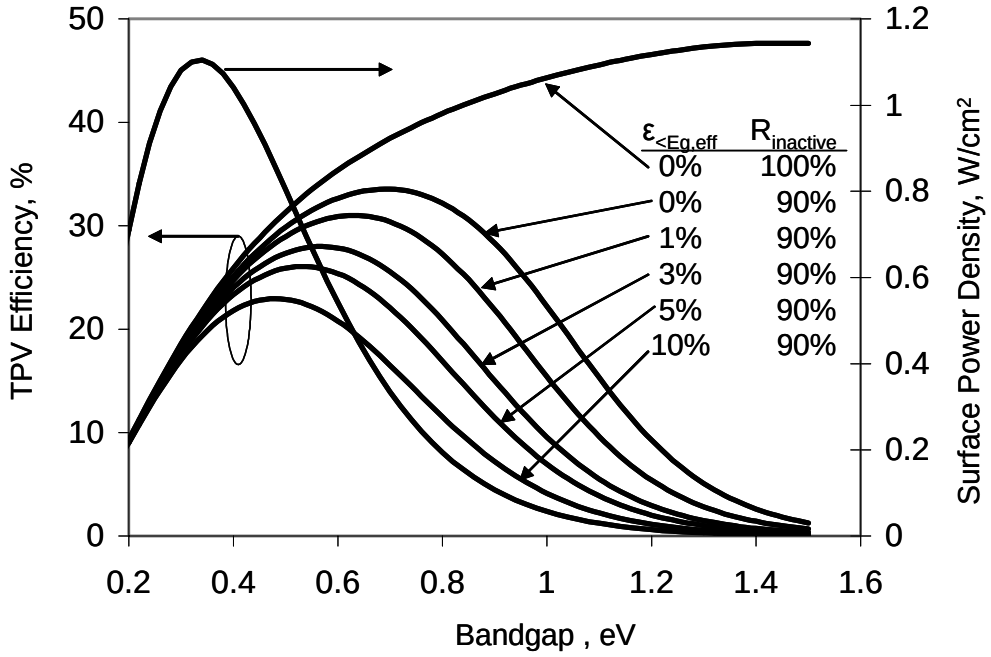

Figure 16: TPV efficiency and power density versus TPV cell bandgap

The importance of band gap on efficiency enters via the determination of the fraction of usable energy (for a given radiator temperature), which subsequently affects spectral efficiency (Figure 6). The strong dependence of TPV efficiency on spectral performance for TPV cell band gaps greater than ~0.4 eV is a result of the relatively low fraction of above band gap photons. It is a key conclusion that lower band gap TPV cells can enable both higher power density and higher efficiency when spectral control limitations are included. In addition, spectral control performance plays a major role in defining the TPV cell band gap that provides the peak TPV

efficiency. In effect, spectral performance (recuperation) in TPV systems is important and for a given radiator temperature influences the determination of the TPV cell band gap.

Spectral Control Influence on TPV Enclosure/Cavity Design

TPV system design introduces unique photonic issues, which affect efficiency and power density. For example, a TPV converter necessarily involves some sort of cavity (Reference (42)). From a photonic viewpoint, the key TPV cavity attributes are:

1. parasitic absorption at inactive cold side areas (e.g., grids, busbars, and gaps between TPV cells)
2. angular and polarization dependent radiator emissivity (i.e., non-Lambertian),
3. angular and polarization dependent front surface filter reflectivity
4. finite separation between radiator and TPV cell which alters the angular dispersion
5. cavity edge leakage or sidewall absorption

These non-ideal cavity attributes complicate the photon recuperation process. In general, advanced numerical techniques such as Monte Carlo and photon ray tracing are needed to quantify the impact of these processes on TPV performance (Reference (42, 43)).

The impact of parasitic absorption in inactive cold side areas on TPV efficiency can be quantified via a module efficiency factor, η_{module}. The module efficiency factor is directly proportional to TPV efficiency and is defined as the total photonic energy absorbed in active TPV cell area divided by total photonic energy absorbed. Figure 17 shows the results of a simplified cavity analysis that examines the impact of inactive area and its reflectivity (assumed to be constant with wavelength and incident angle) on η_{module}. This analysis is based on the following assumptions:

- $\varepsilon_{rad}(\lambda,\theta) = 0.9$
- use of a front surface filter with
    - integrated above band gap filter reflection = 15%
    - integrated above band gap filter parasitic absorption = 2%
- T_h = 1750F
- E_g = 0.5 eV

As shown in Figure 17, both the fraction of active area and the reflectivity of inactive area ($R_{inactive}$) have a strong influence on module efficiency; for example, 85% active area and 90% inactive area reflectivity results in η_{module}~0.9. Figure 18 shows η_{module} versus inactive area reflectivity for TPV cell bandgaps of 0.4, 0.5, 0.6, and 0.7 eV assuming 85% active area. As shown in Figure 18, η_{module} is also a strong function of the TPV cell bandgap with higher cell bandgaps resulting in lower module efficiency. This result is expected since the TPV cell bandgap plays a major role in determining the total photonic energy absorbed, but does not impact parasitic absorption in the inactive area. The large variation in module efficiency shown in Figure 17 and Figure 18 indicates the importance of including cavity photonic issues when estimating TPV system performance.

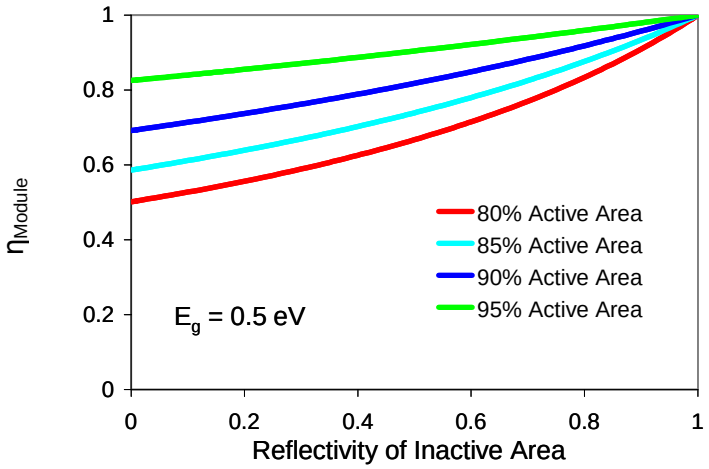

Figure 17: Module efficiency versus inactive area reflectivity and active area fraction

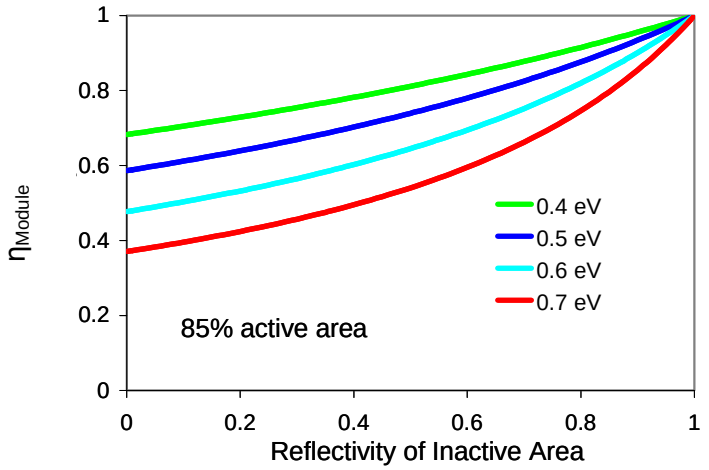

Figure 18: Module efficiency versus inactive area reflectivity and TPV cell bandgap

CONCLUSIONS

Front surface, tandem filters coupled with a high emissivity (~0.8) radiator have achieved the highest spectral performance for thermophotovoltaic energy conversion systems. The other, lower performing TPV spectral control options shown in Table 1 may have applications where front surface, tandem filters are unsuitable or radiating power needs to be adjusted or controlled as with a radioisotope, heat-to-electricity conversion system. To compare these technologies, the relative performance of each TPV spectral control option is shown in Table 3.

Table 3: Relative Performance of TPV Spectral Control Options

Above Band Gap Transmission	Spectral Efficiency: Low	Medium	High
Low	**FSS Filters**		
Medium	**Radiators**		**Tandem Filters**
High		**Back Surface Reflectors**	

Various combinations of these spectral control technologies can in some cases be used together to further improve performance.

Key technical conclusions include:

- Spectral control performance is important for TPV cell performance in a TPV system and influences the optimum bandgap for a given radiator temperature.
- Low bandgap TPV cells are conceptually enabling for both higher TPV efficiency and higher power density when spectral control limitations are included.
- Front surface tandem filters have achieved the highest spectral control performance for TPV energy conversion.
- Higher performance for front surface, frequency selective surface (FSS) filters is limited due to finite conductivity of the metal used to create the surface. Therefore, FSS filters do not satisfy the strict requirements for high spectral efficiency and high above band gap transmission as compared to current tandem filter technology.
- Back surface reflectors have achieved useful levels of spectral performance but less than the spectral performance of tandem filters. Higher performance for back surface reflectors is limited by free carrier absorption in the TPV cell layers.
- The spectral performance of radiator materials for TPV spectral control lags the performance of front surface, tandem filters for energy conversion in an application requiring maximum power density.

REFERENCES

[1] L. D. Woolf, "Solar photothermophotovoltaic energy conversion," presented at IECEC '87; Proceedings of the Twenty-second Intersociety Energy Conversion Engineering Conference, Philadelphia, PA; UNITED STATES, 1987.

[2] L. D. Woolf, D. M. Duggan, and J. Joe N Smith, "Variable band gap materials for thermophotovoltaic generators (Final Technical Report)," GA Technologies, Inc., San Diego, CA. 1987.

[3] L. G. Ferguson and F. Dogan, "A Highly Efficient NiO-Doped MgO Matched Emitter for Thermphotovoltaic Energy Conversion," *Materials Science and Engineering B*, vol. 83, pp. 35-41, 2001.

[4] L. G. Ferguson and F. Dogan, "Spectral Analysis of Transition Metal-Doped MgO "Matched Emitters" for Thermophotovoltaic Energy Conversion," *Journal of Materials Science*, vol. 37, pp. 1301-1308, 2002.

[5] B. S. Good, D. A. Chubb, and A. Pal, "Temperature Gradient Effects in an Erbium Aluminum Garnet Selective Emitter," in *Thermophotovoltaic Generation of Electricity: Fourth NREL Conference*, T. J. Coutts, J. B. Benner, and C. S. Allman, Eds. Woodbury, N.Y.: The American Institute of Physics, 1999, pp. 214-223.

[6] A. Heinzel, V. Boerner, A. Gombert, V. Wittwer, and J. Luther, "Microstructured Tungsten Surfaces as Selective Emitters," in *Thermophotovoltaic Generation of Electricity: Fourth NREL Conference*, T. J. Coutts, J. B. Benner, and C. S. Allman, Eds. Woodbury, N.Y.: The American Institute of Physics, 1999, pp. 191-195.

[7] D. E. Pierce and G. Guazzoni, "High temperature optical properties of thermophotovoltaic emitter components," in *Thermophotovoltaic Generation of Electricity: Fourth NREL Conference*, T. J. Coutts, J. B. Benner, and C. S. Allman, Eds. Woodbury, N.Y.: The American Institute of Physics, 1999, pp. 177-189.

[8] M. F. Rose, P. Adair, and K. Schroeder, "Selective Emitters for Thermophotovoltaic Power Systems for Use in Aerospace Applications," *Journal of Propulsion and Power*, vol. 12, pp. 83-88, 1996.

[9] A. Sentenac and J.-J. Greffet, "Design of Surface Microrelief with Selective Radiative Properties," *International Journal of Heat and Mass Transfer*, vol. 37, pp. 553-558, 1994.

[10] L. Fraas, J. Avery, E. Malfa, J. G. Wuenning, G. Kovacik, and C. Astle, "Thermophotovoltaic for Combined Heat and Power Using Low NOx Gas Fired Radiant Tube Burners," in *Thermophotovoltaic Generation of Electricity: Fifth Conference*, T. J. Coutts, G. Guazzoni, and J. Luther, Eds. Melville, N.Y.: The American Institute of Physics, 2003.

[11] C. J. Crowley, N. A. Elkouh, and P. J. Magari, "Thermal Spray Approach for TPV Emitters," in *Thermophotovoltaic Generation of Electricity: Fourth NREL Conference*, T. J. Coutts, J. B. Benner, and C. S. Allman, Eds. Woodbury, N.Y.: The American Institute of Physics, 1999, pp. 197-213.

[12] S.-Y. Lin, J. Moreno, and J. G. Fleming, "Three-Dimensional Photonic-Crystal Emitter for Thermo Photovoltaic Power Generation," *Applied Physics Letters*, vol. 83, pp. 380-382, 2003.

[13] K. Jarefors, L. Broman, and J. Marks, "Optical Interference Filters in Thermophotovoltaic Applications," in *Thermophotovoltaic Generation of Electricity: Fourth NREL Conference*, T. J. Coutts, J. B. Benner, and C. S. Allman, Eds. Melville, N.Y: The American Institute of Physics, 1999, pp. 390-392.

[14] U. Ortabasi and B. Bovard, "Rugate Technologye for Thermophotovoltaic (TPV) Applications: A New Approach to Near Perfect Filter Performance," in

Thermophotovoltaic Generation of Electricity: Fifth Conference, T. J. Coutts, G. Guazzoni, and J. Luther, Eds. Melville, N.Y.: The American Institute of Physics, 2003, pp. 241-248.

[15] C. F. Hickey, M. Trahan-Verma, and D. M. DePoy, "Antimony Selenide in Multilayer Coatings," in *Optical Interference Coatings*, T. J. Coutts, J. B. Benner, and C. S. Allman, Eds.: Optical Society of America, 2001, pp. ThE4-1, ThE4-3.

[16] D. M. DePoy, R. J. Dziendziel, G. W. Charache, P. F. Baldasaro, and B. C. Campbell, "Interference Filters for Thermophotovoltaic Applications," in *Optical Interference Coatings*, vol. 9: Optical Society of America, 1998, pp. ThC5-1, ThC5-2.

[17] L. M. Fraas, J. E. Samaras, P. F. Baldasaro, and E. J. Brown, "Spectral Control for Thermophotovoltaic Generators (US Patent 5,403,405)." USA: JX Crystals, Inc., 1993.

[18] B. Munk, *Frequency Selective Surfaces*. New York: John Wiley and Sons, 2000.

[19] P. M. Fourspring, D. M. DePoy, H. Ehsani, J. J. Azarkevich, E. J. Brown, S. R. Burger, T. A. Lavery, P. C. Sander, T. D. Rahmlow Jr., J. E. Lazo-Wasem, and E. J. Gratrix, "Recent TPV Spectral Control Development Results," presented at Direct Energy Conversion Technology (DTEC), 2006.

[20] P. F. Baldasaro, J. E. Raynolds, G. W. Charache, D. M. DePoy, C. T. Ballinger, T. Donovan, and J. M. Borrego, "Thermodynamic Analysis of Thermophotovoltaic Efficiency and Power Density Tradeoffs," *Journal of Applied Physics*, vol. 89, pp. 3319-3327, 2001.

[21] B. Wernsman, R. R. Siergiej, S. D. Link, R. G. Mohorter, M. N. Palmisiano, R. J. Wehrer, R. W. Schultz, G. P. Schmuck, R. L. Messham, S. Murray, C. S. Murray, F. Newman, D. Taylor, D. M. DePoy, and J. Thomas D. Rahmlow, "Greater than 20% Radiant Heat Conversion Efficiency of a Thermophotovoltaic Radiator / Module System Using Reflective Spectral Control," *IEEE Transactions on Electron Devices*, vol. 51, pp. 512-515, 2004.

[22] T. D. Rahmlow Jr., J. E. Lazo-Wasem, E. J. Gratrix, P. M. Fourspring, and D. M. DePoy, "New Performance Levels for TPV Front Surface Filters," presented at 6th International Conference on the Thermophotovoltaic Generation of Electricity (TPV6), Frieburg, Germany, 2004.

[23] P. M. Fourspring, D. M. DePoy, J. F. Beausang, E. J. Gratrix, R. T. Kristensen, T. D. Rahmlow, Jr., P. J. Talamo, J. E. Lazo-Wasem, and B. Wernsman, "Thermophotovoltaic Spectral Control," presented at 6th International Conference on the Thermophotovoltaic Generation of Electricity (TPV6), Frieburg, Germany, 2004.

[24] P. M. Fourspring, D. M. DePoy, T. D. Rahmlow, Jr., J. E. Lazo-Wasem, and E. J. Gratrix, "Optical Coatings for Thermophotovoltaic Spectral Control," presented at Optical Interference Coatings, Tucson, Az, 2004.

[25] R. T. Kristensen, J. F. Beausang, and D. M. DePoy, "Frequency Selective Surfaces as Near Infrared Electro-Magnetic Filters for Thermophotovoltaic Spectral Control," *Journal of Applied Physics*, vol. 95, pp. 4845-4851, 2004.

[26] T. D. Rahmlow Jr., J. E. Lazo-Wasem, E. J. Gratrix, J. J. Azarkevich, E. J. Brown, D. M. DePoy, D. R. Eno, P. M. Fourspring, J. R. Parrington, R. G. Mahorter, and B. Wernsman, "Engineering Spectral Control Using Front Surface Filters for Maximum TPV Energy Conversion System Performance," presented at International Energy Conversion Engineering Conference, Providence, RI, USA, 2004.

[27] J. Raynolds, G. W. Charache, C. B. Geller, F. H. Pollack, R. Asahi, and A. J. Freeman, "Theoretical prediction of the plasma frequency and moss-burstein shifts for

degenerately doped InAs, InGaAs, and InPAs," presented at Thermophotovoltaic Generation of Electricity, 1999.

[28] G. W. Charache, D. M. DePoy, J. E. Raynolds, P. F. Baldasaro, K. E. Mihano, T. Holden, F. H. Pollack, P. R. Sharps, M. L. Timmons, C. B. Geller, W. Mannstadt, R. Asahi, A. J. Freeman, and W. Wolf, "Moss-Burstein and Plasma Reflection Characteristics of Heavily-Doped N-type InGaAs and InPAs," *Journal of Applied Physics*, vol. 86, pp. 452, 1999.

[29] B. Wernsman, R. G. Mahorter, R. R. Siergiej, S. D. Link, R. J. Wehrer, S. J. Belanger, P. M. Fourspring, S. Murray, F. Newman, D. R. Taylor, and T. D. Rahmlow Jr., "Advanced Thermophotovoltaic Devices for Space Nuclear Power Systems," presented at Space Technology and Applications International Forum - STAIF 2005, New Mexico, USA, 2005.

[30] W. E. Horne and M. D. Morgan, "Filter Array for Modifying Radiant Thermal Energy," 1997.

[31] W. E. Horne, M. D. Morgan, and V. S. Sundaram, "IR Filters for TPV Converter Modules," in *The Second NREL Conference on Thermophotovoltaic Generation of Electricity*, J. P. Benner, T. J. Coutts, and D. S. Ginley, Eds. Woodbury, N.Y.: AIP Press, 1996, pp. 35-51.

[32] T. K. Wu, "Infrared Filters for High Efficiency Thermophotovoltaic Devices," *Microwave and Optical Technology*, vol. 15, pp. 9-12, 1997.

[33] S. J. Spector, D. K. Astolfi, S. P. Doran, T. M. Lyszczarz, and J. E. Raynolds, "Infrared Frequency Selective Surfaces Fabricated Using Optical Lithography and Phase Shift Masks," *Vacuum Science Technology*, vol. B, pp. 2757-2760, 2001.

[34] E. Topsakal and J. L. Volakis, "On the Properties of Materials for Designing Filters at Optical Frequencies," presented at 2003 IEEE AP-S International Symposium and URSI National Radio Science Meeting, 2003.

[35] J. B. Pryor, "On Ohmic Losses in Frequency Selective Surfaces at Near-Infrared Wavelengths," in *Electrical Engineering*: Ohio State University, 2003.

[36] M. B. Clevenger, C. S. Murray, S. A. Ringel, R. N. Sachs, L. Qin, and D. M. DePoy, "Optical Properties of Thin Semiconductor Device Structures with Reflective Back Surface Layers," presented at Thermophotovoltaic Generation of Electricity, 1999.

[37] G. W. Charache, D. M. DePoy, P. F. Baldasaro, and B. C. Campbell, "Thermophotovoltaic Devices Utilizing a Back Surface Reflector for Spectral Control," presented at Thermophotovoltaic Generation of Electricity, 1995.

[38] Iles and Chu, "TPV Cells with High BSR," presented at Thermophotovoltaic Generation of Electricity, 1995.

[39] M. W. Wanlass, "Advanced High Efficiency Concentrator Solar Cells," presented at 22nd IEEE Photovoltaic Specialists Conference, 1991.

[40] M.W.Dashiell, et al, "0.52eV Quaternary InGaAsSb Thermophotovoltaic Diode Technolog," presented at Sixth Conference on Thermophotovoltaic Generation of Electricity, 2004.

[41] P. Asbeck, "Self-absorption effects on the radiative lifetime in GaAs-GaAlAs double heterostructures," *Journal of Applied Physics*, vol. 48, pp. 820, 1977.

[42] C. K. Gethers, C. T. Ballinger, M. A. Postlethwait, D. M. DePoy, and P. F. Baldasaro, "TPV Efficiency Predictions and Measurements for a Closed Cavity Geometry," presented at Thermophotovoltaic Generation of Electricity, 1995.

[43] C. T. Ballinger, G. W. Charache, and C. S. Murray, ""Monte-Carlo Analysis of Monolithic Interconnected Module with a Back Surface Reflector," in *Thermophotovoltaic*

Generation of Electricity: Fourth NREL Conference, T. J. Coutts, J. B. Benner, and C. S. Allman, Eds. Woodbury, N.Y.: The American Institute of Physics, 1999, pp. 161.